PERGAMON

International Journal of Solids and Structures 40 (2003) 4043–4069

INTERNATIONAL JOURNAL OF SOLIDS and STRUCTURES

www.elsevier.com/locate/ijsolstr

Global–local analysis of granular media in quasi-static equilibrium

K. Kaneko [a], K. Terada [b,*], T. Kyoya [b], Y. Kishino [b]

[a] *Department of Environmental and Civil Engineering, Hachinohe Institute of Technology, Hachinohe 031-8501, Japan*
[b] *Department of Civil Engineering, Tohoku University, Aoba-ku, Sendai 980-8579, Japan*

Received 20 December 2001; received in revised form 10 March 2003

Abstract

A method of global–local analysis is developed for quasi-static equilibrium problems for granular media. The two-scale modeling based on mathematical homogenization theory enables us to formulate two separate boundary value problems in terms of macro- and microscales. The macroscale problem governs the equilibrium of a global structure composed of granular assemblies, while the microscale one is posed for the particulate nature of a local structure with the friction-contact mechanism between particles. The local structure is identified with a periodic representative volume element, or equivalently, a unit cell, over which averaging is performed. The mechanical behavior of unit cells is analyzed by a discrete numerical model, in which spring and friction devices connect rigid particles, whereas the continuum-based finite element method is used for the macroscopic one. Representative numerical examples are presented to demonstrate the capability of the proposed two-scale analysis method for granular materials.

Keywords: Global–local analysis; Granular media; Two-scale modeling; Homogenization method

1. Introduction

Granular media such as sands and powders are regarded as composite materials that reveal fine scale heterogeneities. The recognition common to their mathematical modeling is that the local region is occupied by small particles, while it is identified with a material point in the overall structure. Since the materials have such two-scale nature, the characterization of the mechanical behavior of granular media intrinsically involves two distinct scales, namely micro- and macroscales, and invites two separate modeling approaches. One of them is the macroscopic one that commonly leads to the construction of continuum-based phenomenological constitutive models. The other is the microscopic modeling that tries to capture the particulate or discrete nature of a granular medium within the framework of micromechanics. The former can

* Corresponding author. Tel.: +81-22-217-7417; fax: +81-22-217-7127.
E-mail address: tei@civil.tohoku.ac.jp (K. Terada).

0020-7683/03/$ - see front matter © 2003 Elsevier Science Ltd. All rights reserved.
doi:10.1016/S0020-7683(03)00209-9

predict the mechanical behavior of an overall or global structure with reasonable reality, whereas the latter is useful to characterize the macroscopic material behavior from the microscopic point of view.

Although the macroscopic modeling often enables us to simulate the overall responses of granular media successfully, the aforementioned two-scale nature is central to the studies with the microscopic modeling as in micromechanics, in which the macroscopic material characteristics are described by means of averaging schemes. Some of them try to derive the analytical form of constitutive relations for granular media and others make discussion with reference to the numerical solutions obtained from discrete numerical models.

There seem several theoretical studies that incorporate the microscale particulate mechanism into the macroscopic stress–strain relationship (Emeriault et al., 1996; Liao et al., 2000; Nemat-Nasser, 2000). Although these studies try to model the macroscopic stress–strain relationship by averaging the local variables such as the velocity of each particle and the contact force, and by using the local constitutive law, the complex deformation characteristics of granular media seems still far from being fully understood.

On the contrary, there have been many studies referring to numerical solutions, which can be obtained by discrete numerical models. The distinct element method (DEM), which was proposed by Cundall and Strack (1979), is one of the most popular discrete models. The DEM can be utilized to characterize the macroscopic elastic–plastic mechanical behavior of a granular assembly, but is suited mainly for dynamic motions. For the quasi-static equilibrium states of granular media, Kishino (1989) developed the granular element method (GEM) to study the flow rule and the stability conditions for granular media: see also Wren and Borja (1997) and Kuhn (1999) who utilized numerical methods similar to the GEM to study the macroscopic constitutive laws for granular media.

From the engineering point of views, both the computational and theoretical studies would eventually lead to the development of constitutive equations (macroscopic stress–strain relationships), and hopefully provide the reasonable approximation of the material characteristics that possess the two-scale nature of granular media. However, it is indeed a formidable task when the mathematical consistency is further required within the framework of calculus of variations. Inevitably therefore, little attention has been given to the global–local simulation for the boundary value problem of the overall continuum body with discrete treatment of granular assemblies.

On the other hand, the mathematical theory of homogenization for heterogeneous media with periodic microstructures enables us to realize the two-scale modeling, which consistently entails both micro- and macroscales together with variational statements (see, e.g., Sanchez-Palencia, 1980; Lions, 1981; Benssousan et al., 1978). Due to such consistency, the nonlinear mechanical behavior is easily incorporated into the numerical analysis by the finite element method (FEM) (see, e.g., Swan and Cakmak, 1994; Ghosh and Moorthy, 1995). Recently, Terada and Kikuchi (2001) have originally proposed the consistent two-scale modeling for nonlinear problems by using the generalized convergence theorems in the nonlinear homogenization theory and developed the two-scale or global–local analysis method, which enables us to successfully simulate the macroscopic inelastic behavior induced by the microscale structural responses. Such capability can be attained neither by the theoretical counterparts nor the experimental studies. The modeling strategy has not been applied to the characterization of mechanical behavior of granular media so far.

In this study, we propose a method of global–local analysis for granular materials with reference to Terada and Kikuchi (2001). The problem can be formulated in terms of two distinct scales; macro- and microscales. The former scale defines a global structure, the latter a local structure or equivalently a representative volume element (RVE). The macroscopic field variables are simply calculated as the volume average of the corresponding microscopic ones over the RVE and meet quasi-static equilibrium of an overall structure. On the other hand, the particulate nature with friction-contact behavior is given to the RVE in a microscale. The RVE is assumed to be periodic throughout the paper and is often rephrased as a unit cell. Then, the derived two-scale boundary value problem allows us to analyze the microscale behavior of unit cells by the GEM (Kishino, 1989), in which spring and friction devices connect rigid particles with each other, while the macroscopic problem is solved by the continuum-based FEM.

In Section 2, we pose the two-scale boundary value problem within the framework of homogenization. Section 3 is devoted to the solution scheme of our proposed global–local analysis method, into which the GEM is incorporated. We summarize the analysis procedure and provide the concrete numerical algorithm, whereas the details of the GEM are worked out in Appendix A. In Section 4, we examine the characteristics of the assemblies of particles (circular disks), and then present two representative numerical examples to demonstrate the performance of the proposed global–local analysis method. One of them is a numerical simulation of bi-axial compression tests for noncohesive granular media and the other is a bending test simulation of a beam-like structure composed of cohesive particles. The intimate relationship between the microscopic deformation mechanisms in unit cells and the macroscopic mechanical behavior is illustrated in a numerical manner. Then, we discuss the applicability of the proposed method as well as its limitation.

2. Two-scale modeling of granular materials

We consider the quasi-static boundary value problem of a granular body shown in Fig. 1(a). The body is regarded as an assembly of periodic arrangements of basic microstructural elements (called unit cells), which are composed of a random distribution of elastic particles and voids (see Fig. 1(b)). It is assumed that the problem can be defined in two-dimension (plane strain) and the particles are idealized to be circular. We also assume that the size of a unit cell is small enough to the overall structure and is represented by a normalized parameter ε.

2.1. Variational formulation of friction-contact problem

Let Ω^ε be an open domain of the granular body with smooth boundary $\partial\Omega^\varepsilon$, and divided into three parts as follows:

$$\Omega^\varepsilon = \Omega^\varepsilon_{\mathrm{P}} \cup \Omega^\varepsilon_{\mathrm{V}} \cup C^\varepsilon, \tag{1}$$

where $\Omega^\varepsilon_{\mathrm{P}}$ is an open domain of particles, $\Omega^\varepsilon_{\mathrm{V}}$ is an open domain of voids and C^ε is the totality of the internal surfaces associated with contact and friction. We also define partial open domain Ω^ε_C by excluding C^ε from Ω^ε, i.e. $\Omega^\varepsilon_C = \Omega^\varepsilon \setminus C^\varepsilon = \Omega^\varepsilon_{\mathrm{P}} \cup \Omega^\varepsilon_{\mathrm{V}}$. Then, this problem is fully described by the equilibrium problem in Ω^ε_C with $\partial\Omega^\varepsilon$ and friction and contact conditions on C^ε.

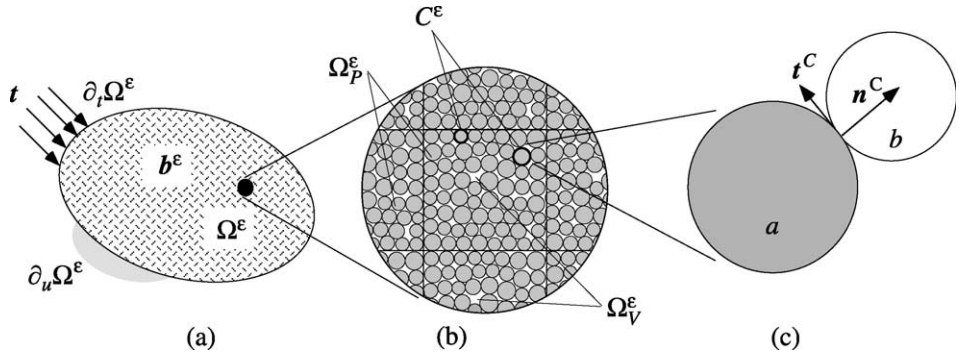

Fig. 1. A body composed of particles (circular disks): (a) macrostructure, (b) microstructure and (c) contact particles.

The equilibrium equation for the stress $\boldsymbol{\sigma}^{\varepsilon}(\boldsymbol{x})$ in Ω_C^{ε} and boundary conditions on $\partial_u\Omega^{\varepsilon} \subset \partial\Omega^{\varepsilon}$ and $\partial_t\Omega^{\varepsilon} \subset \partial\Omega^{\varepsilon}$, which is an external surface of this body, are respectively given by

$$\operatorname{div}\boldsymbol{\sigma}^{\varepsilon}(\boldsymbol{x}) + \boldsymbol{b}^{\varepsilon}(\boldsymbol{x}) = \boldsymbol{0} \text{ in } \Omega_C^{\varepsilon}, \tag{2}$$

$$\boldsymbol{u}^{\varepsilon} = \boldsymbol{0} \text{ on } \partial_u\Omega^{\varepsilon} \quad \text{and} \quad \boldsymbol{\sigma}^{\varepsilon}\cdot\boldsymbol{n} = \boldsymbol{t} \text{ on } \partial_t\Omega^{\varepsilon}, \tag{3}$$

where $\boldsymbol{u}^{\varepsilon}$ is the displacement vector, $\boldsymbol{b}^{\varepsilon}(\boldsymbol{x})$ is the body force, $\boldsymbol{t}$ is the traction vector specified on $\partial_t\Omega^{\varepsilon}$ with the outward unit normal vector $\boldsymbol{n}$. Here and in the subsequent sections, we indicate the dependency on the microscopic heterogeneities by a superscript ε on each variable. It is also assumed that individual particles and voids reveal elasticity along with the following constitutive equation:

$$\boldsymbol{\sigma}^{\varepsilon}(\boldsymbol{x}) = \boldsymbol{D}^{\varepsilon}(\boldsymbol{x}) : \boldsymbol{e}^{\varepsilon}(\boldsymbol{x}), \tag{4}$$

where $\boldsymbol{e}^{\varepsilon}$ is an infinitesimal strain and $\boldsymbol{D}^{\varepsilon}$ the elasticity tensor, which is symmetric and positive definite (it is 0 in the voids if the body is fully dry). The strain is related to the displacement by the following relationship as usual:

$$\boldsymbol{e}^{\varepsilon}(\boldsymbol{x}) = \nabla^{(\mathrm{S})}\boldsymbol{u}^{\varepsilon}, \tag{5}$$

where $\nabla^{(\mathrm{S})}$ is a gradient operator which produces a symmetric second-order tensor.

In order to provide the complete set of governing equations, we here define the friction and contact conditions on C^{ε}. Fig. 1(c) shows the illustration of these conditions on particle a, on which the outward unit normal $\boldsymbol{n}^C$ and the unit tangential vector $\boldsymbol{t}^C$ are defined so that $(\boldsymbol{n}^C, \boldsymbol{t}^C)$ can be a set of base vectors for the right-hand local coordinate system. Then, the displacement vector $\boldsymbol{u}^{\varepsilon}$ and the stress vector $\boldsymbol{T}^{\varepsilon}$ on C^{ε} are decomposed respectively into their normal and tangential components as follows:

$$\boldsymbol{u}^{\varepsilon} = \left\{u_{\mathrm{n}}^{\varepsilon}, u_{\mathrm{t}}^{\varepsilon}\right\}^{\mathrm{T}} \quad \left(u_{\mathrm{n}}^{\varepsilon} = \boldsymbol{u}^{\varepsilon}\cdot\boldsymbol{n}^C,\ u_{\mathrm{t}}^{\varepsilon} = \boldsymbol{u}^{\varepsilon}\cdot\boldsymbol{t}^C\right), \tag{6}$$

$$\boldsymbol{T}^{\varepsilon} = \left\{T_{\mathrm{n}}^{\varepsilon}, T_{\mathrm{t}}^{\varepsilon}\right\}^{\mathrm{T}} \quad \left(T_{\mathrm{n}}^{\varepsilon} = \boldsymbol{T}^{\varepsilon}\cdot\boldsymbol{n}^C,\ T_{\mathrm{t}}^{\varepsilon} = \boldsymbol{T}^{\varepsilon}\cdot\boldsymbol{t}^C\right). \tag{7}$$

Using these components, we have the contact condition of Kuhn–Tucker form on C^{ε} as

$$-T_{\mathrm{n}}^{\varepsilon} \geqslant 0, \quad [[u_{\mathrm{n}}^{\varepsilon}]] \geqslant 0, \quad -T_{\mathrm{n}}^{\varepsilon}[[u_{\mathrm{n}}^{\varepsilon}]] = 0 \qquad \text{on } C^{\varepsilon}, \tag{8}$$

where $[[\cdot]]$ represents the jump of an argument $\cdot$. Under the assumption that each contact region is small enough, the stress vector $\boldsymbol{T}^{\varepsilon}$ can be constant there. Thus, the Coulomb's friction law is introduced as

$$-\mu T_{\mathrm{n}}^{\varepsilon} + c \geqslant |T_{\mathrm{t}}^{\varepsilon}| \quad \text{on } C^{\varepsilon}, \tag{9}$$

where μ and c are the friction coefficient and the cohesion, respectively.

The quasi-static boundary value problem for a granular medium, whose local structure is composed of discrete particles, is completely described by the equilibrium equations (2)–(5) in Ω_C^{ε} and the constraint conditions (8) and (9) for contact and friction on C^{ε}, respectively. Then, the problem is governed by the following variational inequality (Kikuchi and Oden, 1988):

$$\text{Find} \quad \boldsymbol{u}^{\varepsilon} \in \mathscr{K}^{\varepsilon}(\Omega_C^{\varepsilon}) : a(\boldsymbol{u}^{\varepsilon}, \boldsymbol{v}^{\varepsilon} - \boldsymbol{u}^{\varepsilon}) + j(\boldsymbol{u}^{\varepsilon}, \boldsymbol{v}^{\varepsilon}) - j(\boldsymbol{u}^{\varepsilon}, \boldsymbol{u}^{\varepsilon}) \geqslant l(\boldsymbol{v}^{\varepsilon} - \boldsymbol{u}^{\varepsilon}), \quad \forall \boldsymbol{v}^{\varepsilon} \in \mathscr{K}^{\varepsilon}(\Omega_C^{\varepsilon}), \tag{10}$$

where the bilinear form $a(\cdot,\cdot)$ represents the virtual work of the internal forces, the linear form $l(\cdot)$ that of the external forces and $j(\cdot,\cdot)$ that of the friction forces as

$$a(\boldsymbol{u}^{\varepsilon}, \boldsymbol{v}^{\varepsilon}) = \int_{\Omega_C^{\varepsilon}} \nabla\boldsymbol{v}^{\varepsilon} : \boldsymbol{D}^{\varepsilon} : \nabla\boldsymbol{u}^{\varepsilon}\,\mathrm{d}x, \tag{11}$$

$$l(\boldsymbol{v}^{\varepsilon}) = \int_{\partial_{\mathrm{t}}\Omega^{\varepsilon}} \boldsymbol{t}\cdot\boldsymbol{v}^{\varepsilon}\,\mathrm{d}s + \int_{\Omega_C^{\varepsilon}} \boldsymbol{b}^{\varepsilon}\cdot\boldsymbol{v}^{\varepsilon}\,\mathrm{d}x, \tag{12}$$

$$j(\boldsymbol{u}^{\varepsilon},\boldsymbol{v}^{\varepsilon}) = \int_{C^{\varepsilon}} \mu\left|T_{\mathrm{n}}^{\varepsilon}(\boldsymbol{u}^{\varepsilon})\right|\left|[[v_{\mathrm{t}}^{\varepsilon}]]\right|\mathrm{d}s. \tag{13}$$

Here, we have defined the set of admissible displacement vectors $\boldsymbol{v}^{\varepsilon}$ as

$$\mathscr{K}^{\varepsilon}(\Omega_C^{\varepsilon}) = \left\{\boldsymbol{v}^{\varepsilon} \mid v_i^{\varepsilon} \in \mathscr{V}(\Omega_C^{\varepsilon});\ [[v_{\mathrm{n}}^{\varepsilon}]] \geqslant 0 \text{ a.e. on } C^{\varepsilon}\right\}. \tag{14}$$

This convex cone is actually a subset of the following space:

$$\mathscr{V}^{\varepsilon}(\Omega_C^{\varepsilon}) = \left\{\boldsymbol{v}^{\varepsilon} \mid v_i^{\varepsilon} \in H^1(\Omega_C^{\varepsilon});\ v_i^{\varepsilon} = 0 \text{ a.e. on } \partial_{\mathrm{t}}\Omega^{\varepsilon}\right\}, \tag{15}$$

in which $H^1(\Omega_C^{\varepsilon})$ is the Sobolev space of order one.

2.2. Two-scale boundary value problem

A distinguished idea of the mathematical homogenization theory is the modeling with two distinct scales; macro- and microscales, $\boldsymbol{x}$ and $\boldsymbol{y}$, the latter of which is related to the former as $\boldsymbol{y} = \boldsymbol{x}/\varepsilon$. Due to the introduction of these spatial scales, the domain Ω_C^{ε} composed of particles and voids is divided into Ω measured by the macroscopic variable $\boldsymbol{x}$ and $Y_C = Y \setminus C$ measured by the microscopic one $\boldsymbol{y}$ as follows (see Fig. 2):

$$\Omega_C^{\varepsilon} = \Omega \times Y_C = \left\{(\boldsymbol{x},\boldsymbol{y}) \mid \boldsymbol{x} \in \Omega \subset \mathscr{R}^2,\ \boldsymbol{y} = \boldsymbol{x}/\varepsilon \in Y_C \subset \mathscr{R}^2\right\}, \tag{16}$$

where Y is the microscopic domain and C is the contact region. With this decomposition, all the field variables with superscript ε are redefined as functions of two scale variables, $\boldsymbol{x}$ and $\boldsymbol{y}$, as follows:

$$\begin{cases} \boldsymbol{u}^{\varepsilon}(\boldsymbol{x}) = \boldsymbol{u}(\boldsymbol{x},\boldsymbol{y}), & \boldsymbol{e}^{\varepsilon}(\boldsymbol{x}) = \boldsymbol{e}(\boldsymbol{x},\boldsymbol{y}), \quad \boldsymbol{\sigma}^{\varepsilon}(\boldsymbol{x}) = \boldsymbol{\sigma}(\boldsymbol{x},\boldsymbol{y}), \\ \boldsymbol{b}^{\varepsilon}(\boldsymbol{x}) = \boldsymbol{b}(\boldsymbol{x},\boldsymbol{y}), & \boldsymbol{D}^{\varepsilon}(\boldsymbol{x}) = \boldsymbol{D}(\boldsymbol{x},\boldsymbol{y}), \end{cases} \tag{17}$$

each of which is periodic with respect to $\boldsymbol{y}$, i.e. Y-periodic.

It has been demonstrated in Terada and Kikuchi (2001) that the theory of two-scale convergence of Allaire (1992) can be utilized in the derivation of the two-scale boundary value problem for a heterogeneous

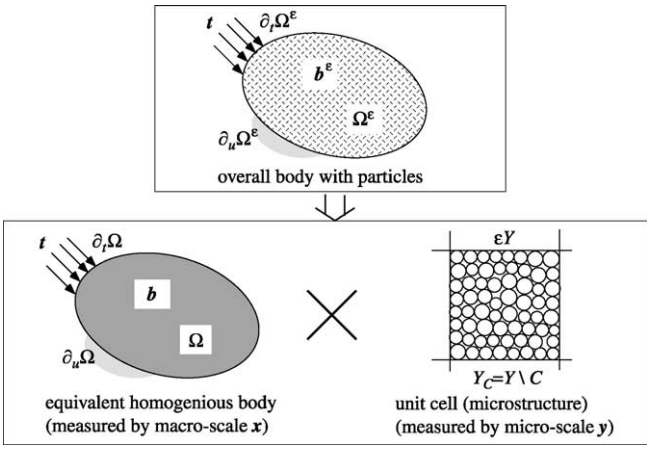

Fig. 2. Decomposition to micro- and macrospace.

solid with periodic microstructures. In this particular situation, the similar argument would hold for the variational inequality (10) and the following formula can be obtained as a limit of the appropriate convergence study:

$$\begin{aligned}&\int_{\Omega}\nabla_x(\boldsymbol{v}^0-\boldsymbol{u}^0):\langle\boldsymbol{D}\rangle:\nabla_x(\boldsymbol{u}^0)\,\mathrm{d}x+\int_{\Omega}\langle\nabla_y(\boldsymbol{v}^1-\boldsymbol{u}^1):\boldsymbol{D}\rangle:\nabla_x(\boldsymbol{u}^0)\,\mathrm{d}x+\int_{\Omega}\nabla_x(\boldsymbol{v}^0-\boldsymbol{u}^0):\langle\boldsymbol{D}:\nabla_y(\boldsymbol{u}^1)\rangle\,\mathrm{d}x\\&+\int_{\Omega}\langle\nabla_y(\boldsymbol{v}^1-\boldsymbol{u}^1):\boldsymbol{D}:\nabla_y(\boldsymbol{u}^1)\rangle\,\mathrm{d}x+\int_C\mu\big|T_{\mathrm{n}}(\boldsymbol{u}^1)\big|\big|[[v_{\mathrm{t}}^1]]\big|\,\mathrm{d}s-\int_C\mu\big|T_{\mathrm{n}}(\boldsymbol{u}^1)\big|\big|[[u_{\mathrm{t}}^1]]\big|\,\mathrm{d}s\\&-\int_{\Omega}\langle\boldsymbol{b}\rangle\cdot(\boldsymbol{v}^0-\boldsymbol{u}^0)\,\mathrm{d}x-\int_{\partial_{\mathrm{t}}\Omega}\boldsymbol{t}\cdot(\boldsymbol{v}^0-\boldsymbol{u}^0)\,\mathrm{d}s\geqslant 0,\quad\forall\boldsymbol{v}^0\in\mathscr{V}\ \text{ and }\ \forall\boldsymbol{v}^1\in\mathscr{K}_{Y_C},\end{aligned}\tag{18}$$

where $\langle\cdot\rangle$ indicates the volume average over the unit cell domain Y, and ∇_x and ∇_y indicate the gradient with respect to the macro- and microscales, respectively. Here, $\boldsymbol{u}^0(\boldsymbol{x})$ and $\boldsymbol{v}^0(\boldsymbol{x})$ are independent of the microscopic heterogeneities and can be chosen from the following admissible functional space on Ω:

$$\mathscr{V}=\big\{\boldsymbol{v}^0(\boldsymbol{x})\mid v_i^0\in H^1(\Omega);\ \ v_i^0=0\ \text{ on }\partial_u\Omega\big\}.\tag{19}$$

On the other hand, the microscopic displacement (trial function) $\boldsymbol{u}^1(\boldsymbol{x},\boldsymbol{y})$ and its variation (test function) $\boldsymbol{v}^1(\boldsymbol{x},\boldsymbol{y})$ are Y-periodic and regarded as elements of the subset $\mathscr{K}_{Y_C}$ of linear space $\mathscr{V}_{Y_C}$, which are respectively given by

$$\mathscr{V}_{Y_C}=\big\{\boldsymbol{v}^1(\boldsymbol{x},\boldsymbol{y})\mid v_i^1\in H^1(\Omega\times Y_C);\ \ Y\text{-periodic}\big\},\tag{20}$$

$$\mathscr{K}_{Y_C}=\big\{\boldsymbol{v}^1(\boldsymbol{x},\boldsymbol{y})\mid\boldsymbol{v}^1\in\mathscr{V}_{Y_C};\ \ [[v_{\mathrm{n}}^1]]\geqslant 0\ \text{ on }C\big\}.\tag{21}$$

Here, one can refer to Allaire (1992) for the relevant definition of two-scale spaces such as $H^1(\Omega\times Y_C)$ and the corresponding convergence studies.

In inequality (18), the test function $\boldsymbol{v}^1$ can be chosen as $\boldsymbol{v}^1=\boldsymbol{u}^1$, while $\boldsymbol{v}^0$ can be chosen as $\boldsymbol{v}^0=\boldsymbol{u}^0+\alpha\boldsymbol{w}^0$ (because $\mathscr{V}$ is a linear space) where $\boldsymbol{w}^0$ is an arbitrary function in $\mathscr{V}$ and α is an arbitrary real number. Then, inequality (18) yields the following equality:

$$\int_{\Omega}\nabla_x(\boldsymbol{w}^0):\big\langle\boldsymbol{D}:\big(\nabla_x(\boldsymbol{u}^0)+\nabla_y(\boldsymbol{u}^1)\big)\big\rangle\,\mathrm{d}x=\int_{\Omega}\langle\boldsymbol{b}\rangle\cdot\boldsymbol{w}^0\,\mathrm{d}x+\int_{\partial_{\mathrm{t}}\Omega}\boldsymbol{t}\cdot\boldsymbol{w}^0\,\mathrm{d}s,\quad\forall\boldsymbol{w}^0\in\mathscr{V}.\tag{22}$$

On the other hand, in inequality (18), $\boldsymbol{v}^0$ can be set to $\boldsymbol{v}^0=\boldsymbol{u}^0$ and $\boldsymbol{v}^1$ to $\boldsymbol{v}^1=\boldsymbol{u}^1+\alpha\boldsymbol{w}^1$. Here, $\boldsymbol{w}^1$ is an arbitrary function in $\mathscr{K}_{Y_C}$ and α is a real number, which is always positive, because the space $\mathscr{K}_{Y_C}$ is a convex cone in this particular setting. Then the variational inequality for $\boldsymbol{u}^1(\boldsymbol{x},\boldsymbol{y})$ in a unit cell yields

$$\begin{aligned}&\int_{Y_C}\nabla_y(\boldsymbol{w}^1):\boldsymbol{D}:\nabla_y(\boldsymbol{u}^1)\,\mathrm{d}y+\int_C\mu\big|T_{\mathrm{n}}(\boldsymbol{u}^1)\big|\big|[[w_{\mathrm{t}}^1]]\big|\,\mathrm{d}s-\int_C\mu\big|T_{\mathrm{n}}(\boldsymbol{u}^1)\big|\big|[[u_{\mathrm{t}}^1]]\big|\,\mathrm{d}s\\&\geqslant-\left(\int_{Y_C}\nabla_y(\boldsymbol{w}^1):\boldsymbol{D}\,\mathrm{d}y\right):\nabla_x(\boldsymbol{u}^0),\quad\forall\boldsymbol{w}^1\in\mathscr{K}_{Y_C},\end{aligned}\tag{23}$$

where the macroscopic deformation $\nabla_x(\boldsymbol{u}^0)$ plays the role of constant excitation. Although the solution of the variational inequality (23) is not unique in $\mathscr{K}_{Y_C}$, it can be unique on the restricted convex cone $\widetilde{\mathscr{K}}_{Y_C}$ which is defined as (Sanchez-Palencia, 1980):

$$\widetilde{\mathscr{K}}_{Y_C}=\big\{\boldsymbol{v}^1(\boldsymbol{x},\boldsymbol{y})\mid\boldsymbol{v}^1\in\mathscr{K}_{Y_C};\ \ \langle\boldsymbol{v}^1\rangle=\boldsymbol{0}\big\}.\tag{24}$$

The average behavior of the overall structure can be characterized by the solution of (22) under the influence of microstructures whose mechanical behavior is characterized by (23). Consequently, the above macroscopic problem has a solution as long as the microscopic problem has a solution, vice versa. These

micro- and macroscopic simultaneous equations govern the two-scale boundary value problem for a granular medium.

2.3. Local (strong) form of the two-scale boundary value problem

The strong forms of the microscopic problem (23) can be identified with

$$\operatorname{div}\boldsymbol{\sigma}^0 = \mathbf{0} \text{ in } Y_C, \tag{25}$$

$$\left.\begin{array}{l} -T_{\mathrm{n}} \geqslant 0, \quad [[u_{\mathrm{n}}^1]] \geqslant 0, \quad -T_{\mathrm{n}}[[u_{\mathrm{n}}^1]] = 0 \\ -\mu T_{\mathrm{n}} + c \geqslant |T_{\mathrm{t}}| \end{array}\right\} \text{ on } C, \tag{26}$$

along with the constitutive equation in a microscale

$$\boldsymbol{\sigma}^0(\boldsymbol{x},\boldsymbol{y}) = \boldsymbol{D} : \left(\nabla_x \boldsymbol{u}^0 + \nabla_y \boldsymbol{u}^1\right) = \boldsymbol{D} : \left(\boldsymbol{E} + \nabla_y \boldsymbol{u}^1\right), \tag{27}$$

where we have defined the macroscopic strain $\boldsymbol{E}$ as

$$\boldsymbol{E} = \nabla_x^{(\mathrm{S})}(\boldsymbol{u}^0). \tag{28}$$

Thus, the actual microscopic displacement vector $\boldsymbol{u}(\boldsymbol{x},\boldsymbol{y})$ is expressed with the macroscopic (average) displacement vector $\boldsymbol{u}^0$ and the Y-periodic microscopic one $\boldsymbol{u}^1(\boldsymbol{x},\boldsymbol{y})$ as

$$\boldsymbol{u}(\boldsymbol{x},\boldsymbol{y}) = \boldsymbol{E}\cdot\boldsymbol{y} + \boldsymbol{u}^1(\boldsymbol{x},\boldsymbol{y}). \tag{29}$$

On the other hand, Eq. (22) is equivalent to the local form of the macroscopic boundary value problem as follows:

$$\operatorname{div}\boldsymbol{\Sigma} + \boldsymbol{B} = \mathbf{0} \text{ in } \Omega, \tag{30}$$

$$\boldsymbol{u}^0 = \mathbf{0} \text{ on } \partial_u\Omega \quad \text{and} \quad \boldsymbol{\Sigma}\cdot\boldsymbol{n} = \boldsymbol{t} \text{ on } \partial_t\Omega. \tag{31}$$

Here, $\boldsymbol{\Sigma}$ and $\boldsymbol{B}$ are the macroscopic stress and the body force, respectively, and are given by the volume averages of the corresponding microscopic variables over a unit cell as

$$\boldsymbol{\Sigma}(\boldsymbol{x}) = \langle\boldsymbol{\sigma}^0(\boldsymbol{x},\boldsymbol{y})\rangle = \langle\boldsymbol{D} : (\boldsymbol{E} + \nabla_y\boldsymbol{u}^1)\rangle, \tag{32}$$

$$\boldsymbol{B}(\boldsymbol{x}) = \langle\boldsymbol{b}(\boldsymbol{x},\boldsymbol{y})\rangle. \tag{33}$$

2.4. General algorithm for global–local computation

In our two-scale modeling based on the mathematical homogenization theory, the boundary value problem for a granular medium is governed by both the macroscopic virtual work equation (22) and the microscopic variational inequality (23). In particular, the Y-periodic microscopic displacement $\boldsymbol{u}^1(\boldsymbol{x},\boldsymbol{y})$ is a solution under the constraint conditions associated with contact and friction. Thus, we note that the governing equations in both scales are completely coupled, but can be solved independently by a sequential solution scheme in each loading step. The general numerical algorithm to solve such two-scale boundary value problems is proposed in Terada and Kikuchi (2001) and is summarized as follows:

(I) With initial macroscopic stress $\boldsymbol{\Sigma}$, solve the macroscopic boundary value problem (22) for macroscopic displacement $\boldsymbol{u}^0(\boldsymbol{x})$.
(II) Evaluate the macroscopic displacement gradient (the macroscopic strain) $\boldsymbol{E} = \nabla_x^{(\mathrm{S})}(\boldsymbol{u}^0)$ at all the macroscopic sampling points.

(III) Using each value of macroscopic strain $\boldsymbol{E}$ as an external force applied to a unit cell, solve the microscopic problem governed by variational inequality (23) for Y-periodic microscopic displacement $\boldsymbol{u}^1(\boldsymbol{x},\boldsymbol{y})$.
(IV) Evaluate microscopic stress $\boldsymbol{\sigma}^0$ from (27) with the values of $\boldsymbol{u}^1(\boldsymbol{x},\boldsymbol{y})$ and $\boldsymbol{E}$.
(V) Compute the new state of macroscopic stress $\boldsymbol{\Sigma}$ by the averaging relation (32).

The processes (I)–(V) are repeated until (22) and (23) are satisfied simultaneously.

This numerical algorithm is general for the materials whose microstructure reveals nonlinearity. Both the macroscopic virtual work equation (22) and the microscopic one can be solved by the continuum-based FEM regardless of the mechanical nature of the microstructure. However, it is generally a tedious task to solve (23) by using the FEM in the case of granular type media because of their discrete nature with friction and contact. Therefore, we identify the physical model assumed in the above formulation, namely, the microstructure composed of elastic particles and voids, with that composed of rigid circular particles, spring elements and frictional devices. This type of physical models is widely used in the single-scale analysis of granular media; e.g., the DEM (Cundall and Strack, 1979). In this paper, we employ the GEM (Kishino, 1989), which can characterize the quasi-static mechanical behavior of an assembly of particles, and work out the detailed formulation in Appendix A.

3. Solution scheme of global–local analysis for granular media

We here outline the solution scheme of the proposed global–local (or two-scale) analysis method for granular media. After defining the macroscopic stress from the GEM context, we recast the discretized version of the two-scale boundary value problems. Then, we summarize the analysis procedure and describe the concrete numerical algorithm for the method.

3.1. Definition of the macroscopic stress in GEM for a unit cell

We consider a unit cell, which is composed of rigid particles (see Fig. 3(a)). In the analysis by the GEM, the macroscopic (average) stress of this granular assembly is represented by the following relationship:

$$\frac{1}{|Y|}\int_Y \boldsymbol{\sigma}^0 \,\mathrm{d}y = \boldsymbol{\Sigma} \approx \frac{1}{|Y|}\sum_E \boldsymbol{T}^E \cdot \boldsymbol{y}^E, \tag{34}$$

where E is the set of contact points on the external boundary ∂Y_C of the unit cell, $\boldsymbol{T}^E$ is the contact force from an external particle to an internal particle, $\boldsymbol{y}^E$ is the position vector of a contact point between the

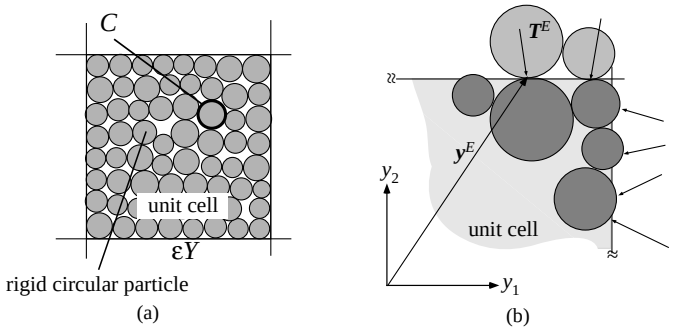

Fig. 3. Unit cell composed of particles: (a) unit cell and (b) force applied by exterior particles.

internal and the external particles, and $|Y|$ is the volume of the unit cell (see Fig. 3(b) and Appendix A for their precise expressions). This definition of average stress is well known in the area of micromechanics for granular materials (see, e.g., Oda and Iwashita, 1999). Indeed, it is recognized that (34) provides a fairly good approximation, though some approximation error is involved. Moreover, the macroscopic stress given by (34) is always symmetric since all the particles within a unit cell satisfy the equilibrium condition for the moment.

3.2. Discretized equations of the global–local boundary value problems

In our solution scheme, the macroscopic problem (22) is analyzed by the standard FEM. In this context, the discretized macroscopic equation can be written as

$$\{\boldsymbol{G}(\boldsymbol{\Sigma})\} = \{\boldsymbol{F}_{\text{ext}}\} \quad \text{in } \Omega \quad \text{[Macroscale problem]} \tag{35}$$

where $\{\boldsymbol{F}_{\text{ext}}\}$ is the external nodal force vector and $\{\boldsymbol{G}(\boldsymbol{\Sigma})\}$ is the internal nodal force vector as a function of the macroscopic stress $\boldsymbol{\Sigma}$, which is evaluated by (34) at each sampling point of an element. Here and in the subsequent sections, the vector and matrix quantities are expressed with $\{\cdot\}$ and $[\cdot]$, respectively.

On the other hand, the incremental form of the microscale stiffness equation, which corresponds to (A.23) in Appendix A, can be written as follows, along with the constraint condition associated with friction and contact in the GEM:

- microscopic stiffness equation

$$\{\Delta\boldsymbol{H}\} = [\boldsymbol{K}]\{\Delta\boldsymbol{u}\} \quad \text{in } Y_C \quad \text{[Microscale problem]}, \tag{36}$$

- constraint conditions ((A.3), (A.4) and (A.6), in order)

$$[[u_{\text{n}}^{ij}]] = 0 \ \text{ on } C^{ij} \in C \quad \text{[contact condition]}, \tag{37}$$

$$|T_{\text{t}}^{ij}| \leqslant -T_{\text{n}}^{ij}\tan\phi \ \text{ on } C^{ij} \in C \quad \text{[friction condition]}, \tag{38}$$

$$\begin{cases} T_{\text{n}}^{ij} \leqslant -c_{\text{n}} \\ |T_{\text{t}}^{ij}| \leqslant -T_{\text{n}}^{ij}\tan\phi + c_{\text{t}} \end{cases} \text{on } C^{ij} \in C \quad \text{[cohesive condition]}. \tag{39}$$

Here, $\{\Delta\boldsymbol{H}\}$ is the increment of the external force vector generated by the macroscopic strain increment $\Delta\boldsymbol{E}$, $[\boldsymbol{K}]$ is the overall stiffness matrix, and $\{\Delta\boldsymbol{u}\}$ is the increment of the overall generalized displacement vector of particles; two translational and one rotational components. Also, $[[u_{\text{n}}^{ij}]]$ is the normal component of the relative displacement in-between particles i and j on a contact point C^{ij}, and T_{n}^{ij} and T_{t}^{ij} are the normal and tangential components of the contact force vector $\{\boldsymbol{T}^{ij}\}$ on C^{ij}, respectively. In addition, ϕ is the friction angle between two particles, and c_{n} and c_{t} are the normal and tangential components of the cohesion, respectively.

Convergence of the iteration in our microscale analysis is achieved when all the particles in a unit cell satisfy the following equilibrium condition, which is equivalent to (A.12):

$$\sum_{j=1}^{\alpha}[\boldsymbol{R}^{ij}]\cdot\{\boldsymbol{T}^{ij}\} = \{\boldsymbol{0}\} \quad \text{in } Y_C \quad (i = 1,\ldots,n). \tag{40}$$

Here, n is the total number of particles in a unit cell, α is the number of particles in contact with particle i, and $[\boldsymbol{R}^{ij}]$ is the coordinate transformation matrix on C^{ij}, as is defined in (A.11). For the microscale analysis in our global–local computations, it is assumed that this equilibrium equation is equivalent to the microscale problem (25). For details of microscale equations (36)–(40) for the GEM see Appendix A or Kishino (1989).

3.3. Numerical algorithm for global–local computations

We here summarize the proposed global–local analysis method, which enables us to simulate the macroscopic mechanical behavior of an overall structure whose microstructure is composed of particles without any complicated constitutive equation for a continuum.

The fundamental concept of the developed global–local analysis method is illustrated in Fig. 4. Here, the macroscale problem is solved by the continuum-based FEM, while the microscale problem is solved by the GEM that provides the macroscopic stress (34). That is, the macroscopic stress is obtained by the microscopic response of a single unit cell to the macroscopic deformation. Due to the nature of such two-scale modeling, this method can be applied regardless of the scale of an overall structure.

Accordingly, the numerical algorithm is basically the same as that described in Section 2 except that the incremental equilibrium states are considered, and that the microscale analysis for a unit cell is performed by the GEM. The analysis flow is presented as follows:

(I) With the values of $\boldsymbol{\Sigma}$, solve the macroscopic boundary value problem (35) for the increment of macroscopic displacement, $\Delta \boldsymbol{u}^0(\boldsymbol{x})$.
(II) Calculate the increment of the macroscopic displacement gradient (the macroscopic strain) $\Delta \boldsymbol{E} = \nabla_x^{(\mathrm{S})}(\Delta \boldsymbol{u}^0)$ at all the macroscopic sampling points.
(III) Using the increment $\Delta \boldsymbol{E} = \nabla_x^{(\mathrm{S})}(\Delta \boldsymbol{u}^0)$ as an external force, perform the microscale analyses for the unit cells located at all the macroscopic sampling (integration) points.
  (i) With the value of $\Delta \boldsymbol{E}$, calculate $\{\Delta \boldsymbol{H}(\Delta \boldsymbol{E})\}$.
  (ii) Solve the quasi-static stiffness equation of the granular assembly (36) for the increment of the overall generalized displacement vector $\{\Delta \boldsymbol{u}\}$.
  (iii) With the value of $\{\Delta \boldsymbol{u}\}$, compute the contact force increment between each particle, and update all the coordinate transformation matrix $[\boldsymbol{R}^{ij}]$ and all the contact force vectors $\{\boldsymbol{T}^{ij}\}$.
  (iv) Check whether or not the contact condition (37), the friction condition (38) and the cohesive condition (39) are satisfied.
  (v) According to the results of (iv), correct the contact force $\{\boldsymbol{T}^{ij}\}$ and check whether or not the equilibrium condition (40) of all the particles is satisfied with corrected $\{\boldsymbol{T}^{ij}\}$ and $[\boldsymbol{R}^{ij}]$.
  (vi) If this condition is not satisfied, go to (i) using the residual force instead of $\{\Delta \boldsymbol{H}(\Delta \boldsymbol{E})\}$.
(IV) Compute the new state of macroscopic stress $\boldsymbol{\Sigma}$ by the averaging relationship (34).

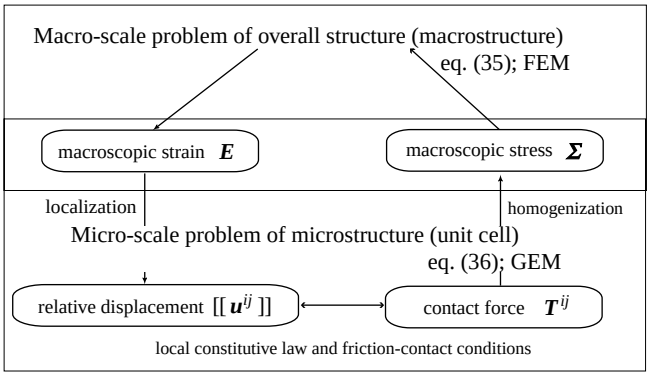

Fig. 4. Concept of two-scale analysis method.

The processes (I)–(IV) is repeated until the micro- and macroscopic equilibrium states are satisfied simultaneously.

4. Representative numerical examples of global–local analyses

We present two representative numerical examples to demonstrate the performance of our proposed method for global–local analyses. One of them is the global–local computation to simulate the bi-axial compression tests of a plane specimen composed of noncohesive granular media. The other is a bending test simulation, which illustrates the effect of cohesion and the irreversible response of an overall structure with granular materials. Prior to these simulations, we first examine the qualification of assemblies of particles (circular disks) to characterize the macroscopic material behavior, which should not depend on the dimensions of unit cells, or equivalently, on the number of particles in a single unit cell.

4.1. Qualification of assemblies of particles for RVE

The qualification of the assemblies of circular particles is examined for RVEs, by which the macroscopic material behavior is evaluated. We first examine the influences of the size and the aspect ratio of unit cells on the characteristics of initial particle arrangements and then on the macroscopic responses.

Unit cell models of 16 different dimensions are prepared and presented in Fig. 5, where the models in Series A and B have aspect ratios of one and two, respectively. We use Model A100 with a dimension of square region $L_1^0 \times L_2^0$ in the figure as a reference, which contains 1600 particles that are randomly generated in the square unit cell region $Y = L_1^0 \times L_2^0$. This reference model has the distribution of particle diameters presented as shown in Fig. 6. The unit cells of all the other models are made smaller than the reference model and their particle arrangements inherit it. In order to conduct the examination below, we introduce the characteristic length as follows:

$$\lambda = \frac{L_1 + L_2}{L_1^0 + L_2^0}, \tag{41}$$

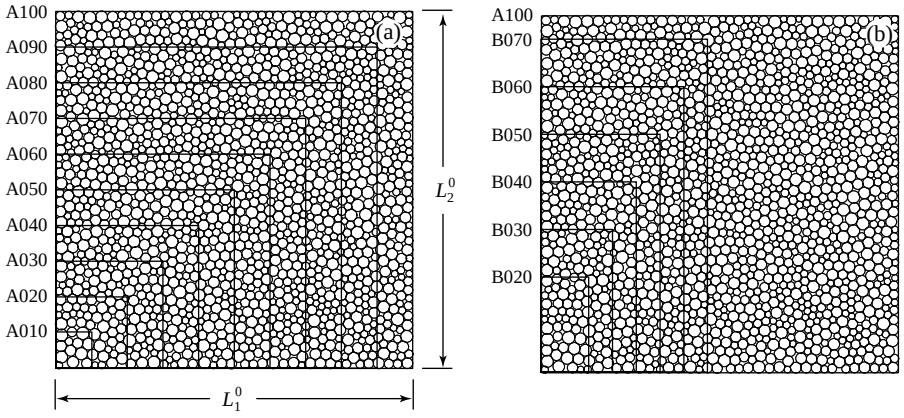

Fig. 5. Unit cell models of different dimensions: (a) Series A (aspect ratio = 1.0) and (b) Series B (aspect ratio = 2.0).

where L_1 and L_2 are respectively the lengths in the y_1- and y_2-directions of each unit cell model. All the models can be identified by this parameter; for example, Model A020 has $\lambda = 0.20$ in Series A, Model B050 has $\lambda = 0.50$ in Series B and so on.

Physical parameters are given as follows: the normal spring constant $s_n = 5.0 \times 10^4$ N/m, the tangential one $s_t = 3.5 \times 10^4$ N/m, the friction angle $\phi = 25°$ and the cohesions $c_n = c_t = 0$ MPa. We set up the initial states of unit cell models with circular disks with confining pressure 0.2 MPa so that all the models have almost the same void ratios.

From the geometrical viewpoint, the isotropy of the unit cell models can be examined by means of the fabric tensor, which is defined as follows:

$$\boldsymbol{\Pi} = \frac{1}{2M} \sum_{i}^{n} \sum_{j}^{\alpha} \boldsymbol{n}^{ij} \otimes \boldsymbol{n}^{ij}, \tag{42}$$

where M is the total number of contact points in the unit cell region Y, α is the total number of particles in contact with particle i, n is the total number of particles in the unit cell, and $\boldsymbol{n}^{ij}$ is the outward unit normal of particle i onto particle j (see, e.g., Oda and Iwashita, 1999, for this definition). The ratio of the principal values, Π_1 and Π_2, of this tensor can be used to measure the extent of anisotropy. If the ratio is equal to unity, i.e., $\Pi_1/\Pi_2 = 1$, then the unit cell is said to be geometrically isotropic. Thus, the deviation from isotropy can be parameterized as $\Pi_1/\Pi_2 - 1$ and is presented in Fig. 7. As can be seen from the figure, the deviation from geometrical isotropy is at most 0.8% when the characteristic length λ of unit cell is larger

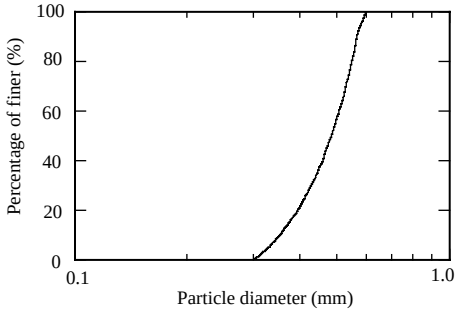

Fig. 6. Accumulation curve for particle size.

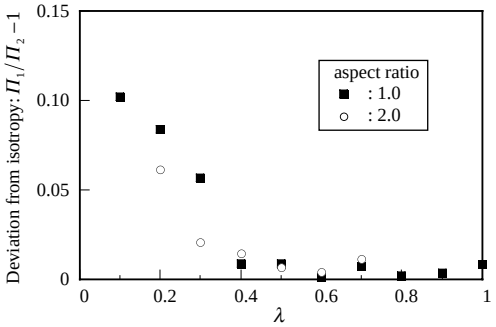

Fig. 7. Deviation from geometrical isotropy for various characteristic lengths.

than 0.4, regardless of aspect ratios. We note here that the models with this value $\lambda = 0.4$ of characteristic length are A040 and B040 and contain about 200 particles in the square region.

In order to examine the influence of the unit cells' dimensions on the macroscopic behavior, we conduct the numerical simulations of the bi-axial tests for each unit cell by imposing the unit macroscopic strain that has either of the following components:

$$\boldsymbol{E}_{\mathrm{V}} = \xi \begin{bmatrix} 1 & 0 \\ 0 & 0 \end{bmatrix} \quad \text{and} \quad \boldsymbol{E}_{\mathrm{H}} = \xi \begin{bmatrix} 0 & 0 \\ 0 & 1 \end{bmatrix},$$

where ξ is the macroscopic loading parameter. Here, the subscripts, V and H, on variables are used to indicate the correspondence to the macroscopically horizontal and vertical loading patterns. Also, we define the following indicators to measure the error due to cell's dimensions and the deviation from mechanical isotropy:

$$\Sigma^{\mathrm{dim}} = \frac{|\overline{S}^0 - \overline{S}|}{\overline{S}^0}, \tag{43}$$

$$\Sigma^{\mathrm{iso}} = \frac{|S_{\mathrm{V}} - S_{\mathrm{H}}|}{\overline{S}}, \tag{44}$$

where

$$S_I = \sqrt{\boldsymbol{\Sigma} : \boldsymbol{\Sigma}} \quad (I = \mathrm{V} \text{ or } \mathrm{H}), \tag{45}$$

$$\overline{S} = (S_{\mathrm{V}} + S_{\mathrm{H}})/2. \tag{46}$$

Here, the S^0 is the norm of the macroscopic stress for Model A100 and the error is evaluated relatively with respect to S^0.

When the parameter ξ becomes 0.01 and 0.03, we calculate these indicators to examine effects of the dimensions of unit cells. Fig. 8 shows the error of the macroscopic stress values due to cells' dimensions and their deviation from mechanical isotropy. Here, the errors and the deviations are relative with respect to that of Model A100 as defined in (43) and (44). As can be seen from each figure, there is an abrupt decrease of the relative error when the characteristic length is 0.3 or 0.4. Especially for the models in Series A, the value at $\lambda = 0.4$ remains less than 5% and thus the unit cell of this characteristic length seems a qualified RVE in evaluating the macroscopic material behavior. Also, even for the models of Series B, which have aspect ratio of 2, the convergence is accomplished when the characteristic length increases. However, the rate of convergence for the deviations from isotropy is slower than that of Series A. In other words, the models of Series B exhibit the anisotropic mechanical behavior prominently as the loading parameter becomes large. This is probably due to the fact that the difference of aspect ratios changes the arrangement of particles differently during the deformation especially when the dimensions of unit cells are relatively small. The confirmation of this conjecture is out of scope of this study, but should be realized in the near future. Nonetheless, it can be expected that, in this particular development, the dimension of the characteristic length at 0.4, which corresponds to the unit cell of about 200 particles, gives practically permissible errors.

4.2. Bi-axial compression tests for noncohesive granular media

4.2.1. Analysis conditions

The finite element model of the macroscopic overall structure under consideration is shown in Fig. 9(a) together with boundary conditions. Here, the displacements on the top and bottom surfaces of length L are

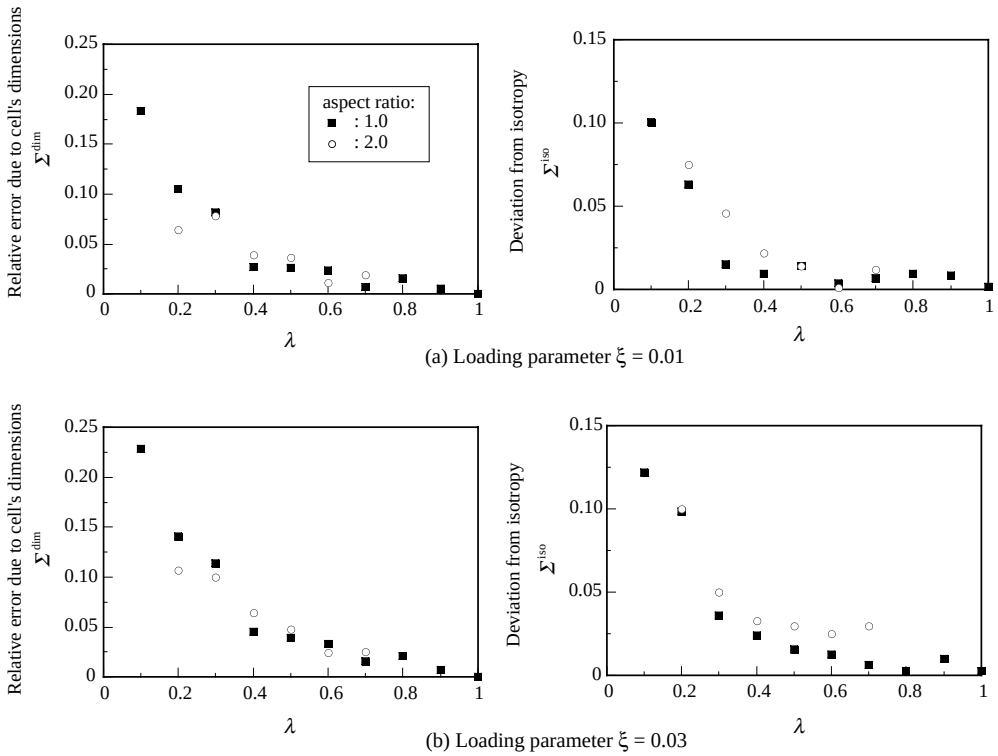

Fig. 8. Relative error of the macroscopic stress values with respect to that of Model A100 and their deviation from isotropy. Loading parameter (a) $\xi = 0.01$ and (b) $\xi = 0.03$.

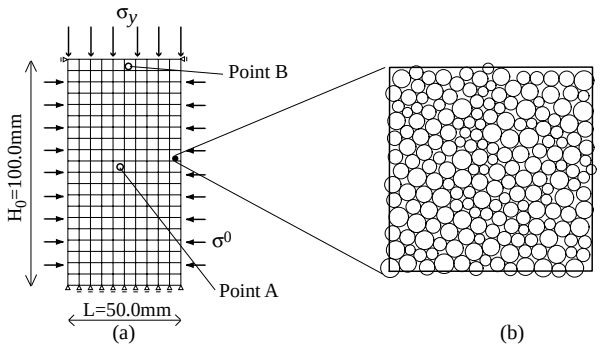

Fig. 9. Macro- and microscopic analysis model: (a) overall macrostructure for FEM and (b) microstructure for GEM.

fixed. The displacement at the top surface is controlled to compress the model for various values of confining pressure; $\sigma^0 = 0.2$, 0.3 and 0.4 MPa. On the other hand, the unit cell model for the microscale granular element analysis is shown in Fig. 9(b), which has about 200 particles and has almost the same characteristics of the distribution of particle diameters as those in Fig. 6. The physical parameters used in the microscopic model are the same as that in Section 4.1.

Before providing the results, we define several physical quantities measured in the following numerical experiments. First of all, the apparent stress and strain for specimens are defined as macroscopic quantities just as those defined in experiments for soils and sands. For example, the axial stress is an apparent quantity, which is evaluated as the nominal stress $\sigma_{\text{axial}} = P/L$ with P being the reaction force at the bottom of the specimen. Thus, the deviator stress is defined as $\sigma_{\text{div}} = \sigma_{\text{axial}} - \sigma^0$. The axial strain is also a macroscopic and apparent quantity defined as $\varepsilon_{\text{axial}} = (\Delta H/H_0) \times 100$ where ΔH is the height change of a specimen with initial height H_0. In view of geotechnical applications, apparent volumetric change called dilatancy is worth to be identified with the volumetric stain $\varepsilon_{\text{vol}} = V/V_0 - 1$ where $V_0 = LH_0$ is the initial volume and V, which is calculated by adding the volume of all elements, is the one after deformation.

4.2.2. Macroscopic deformation characteristics

Fig. 10 shows the relationship between the apparent (macroscopic) deviator stress, σ_{div}, and the axial strain, $\varepsilon_{\text{axial}}$, for various values of confining pressure. As can be seen from this figure, the response is almost linear at the very beginning of loading, and gradually reveals nonlinearity for all the cases. The figure also presents the relationship between the dilatancy characteristics of the specimen and the axial strain. We can see that the compressive loading makes the specimen dilate at the early stage of loading and reach the peak of the curve. In addition, three different stress–strain curves illustrate the pressure dependent behavior, which is known to be peculiar to granular materials. These results seem similar to the ones observed in actual experiments such as tri-axial tests for sands. Note, however, that these measured quantities are apparent ones as mentioned in the above and are not necessarily the same as actual field variables.

The process of the macroscopic deformation under confining pressure $\sigma^0 = 0.3$ MPa is presented in Fig. 11, in which the slack-type deformation is well demonstrated as can be expected. Also, Fig. 12 shows the distributions of the volumetric strain ε_{vol}. Although the dilatancy observed in Fig. 10 is an apparent one for the overall structure, the characteristics recognized from Fig. 12 show that the material itself reveals dilatancy around the center of the specimen when the axial strain reaches 2.0%. In the stage of 2.4% axial strain, material points around the center of the specimen dilate about 0.5% though the overall structure is compressed in the axial direction. This implies that the internal structure of the granular material, i.e., the microstructure, increases its volume. Such behavior of unit cells results from the motion of particles with frictional contact as can be seen later. Thus, the developed two-scale model can reflect the particulate nature in unit cells and reproduce the typical macroscopic deformation characteristics such as the pressure dependency and the dilatancy.

It is, however, difficult to estimate the overall strength of the specimen by the analysis. In this context, Fig. 13 shows the distributions of the semi-norm of the deviator strain under bi-axis compression. As can be seen from the figure, the shear-dominant deformation gradually concentrates around the center of the

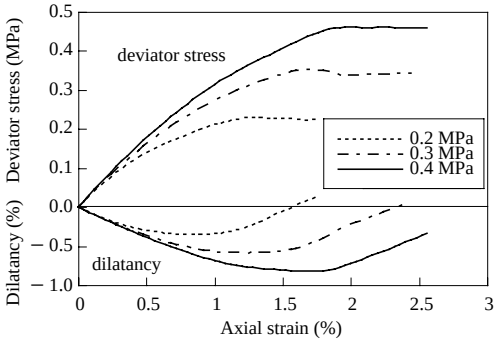

Fig. 10. Stress–strain and dilatancy curves.

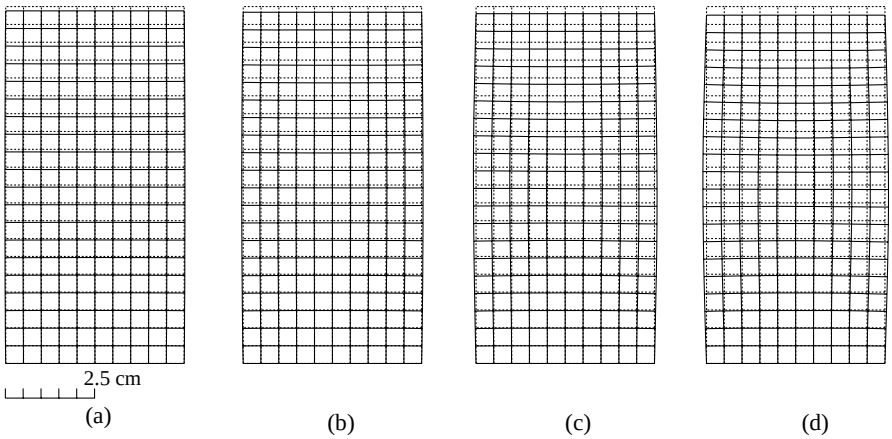

Fig. 11. Macroscopic deformed configuration (initial stress 0.3 MPa). Axial strain (a) 1.2%, (b) 1.6%, (c) 2.0% and (d) 2.4%.

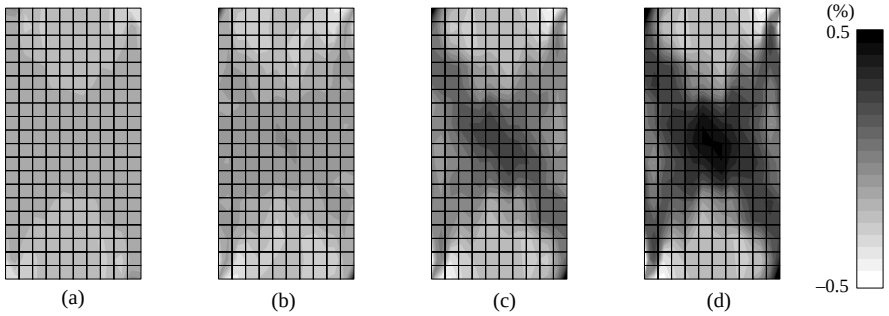

Fig. 12. Distribution of the volumetric strain (initial stress 0.3 MPa). Axial strain (a) 1.2%, (b) 1.6%, (c) 2.0% and (d) 2.4%.

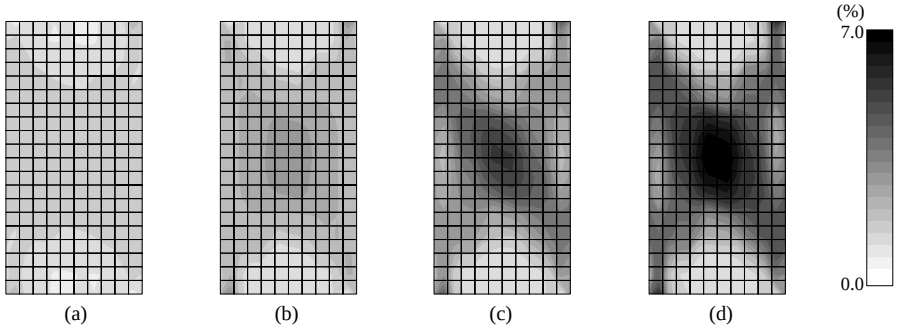

Fig. 13. Distribution of the norm of the deviator strain (initial stress 0.3 MPa). Axial strain (a) 1.2%, (b) 1.6%, (c) 2.0% and (d) 2.4%.

specimen and eventually appears to exhibit the preferable orientation of concentration. Although this is a typical phenomenon observed in compression tests, our global–local computation cannot simulate the formation of a macroscopic slip surface, which leads to overall collapse. In order to characterize such

higher-order nonlinearity, we need to incorporate the nonlocal effects with our two-scale modeling. This subject will be tackled in another opportunity.

4.2.3. Microscopic deformation characteristics

Fig. 14 presents the motion of particles in a unit cells located at macroscopic material points, A and B, which are shown in Fig. 9(a). Here, Point A corresponds to the material point that undergoes large deformation and reveals the concentration of the macroscopic deviator strain, whereas the strain of Point B is comparatively small. As can be seen from the figure, for the cell located at Point A, velocity vectors and rotation rates become large with increasing total loads, though the rate of apparent axial strain of the overall specimen remains constant. On the other hand, for Point B, there is little motion even after the peak of the apparent stress (the apparent axial strain 2.4%).

Fig. 15 shows the distribution of the normal contact forces between particles, which represents the microstructural characteristics, associated with macroscopic material points, A and B. Also, in this figure, a line connecting one particle to another gives the contact force between these mutually connected particles and its thickness represents the magnitude of the force. As can be seen from the figure, the normal contact forces exhibit almost isotropic distribution at the initial state and have the same magnitudes for all material points. This is probably due to the nearly isotropic state of macroscopic stress. In the cell located at Point A, the anisotropic distribution of contact forces gradually evolves with increasing load and becomes the most prominent when the apparent axial strain reaches 2.4% in this particular computation. This induced anisotropic nature of the microscopic response is represented by the relatively thicker lines forming the vertical lines and by the thin ones corresponding to the small forces in the horizontal direction. The vertical direction of the transmission of contact forces coincides with that of the maximum principal axis of the macroscopic apparent stress. As for Point B, the anisotropic distribution, which is similar to that in Point A, was observed. However, the distribution of contact forces seems to remain unchanged throughout the deformation process. Thus, the microstructural characteristics of the cells located at Points A and B differ significantly when the axial strain is 2.4%, though they are similar to each other when the axial strain is small, say 1.0%.

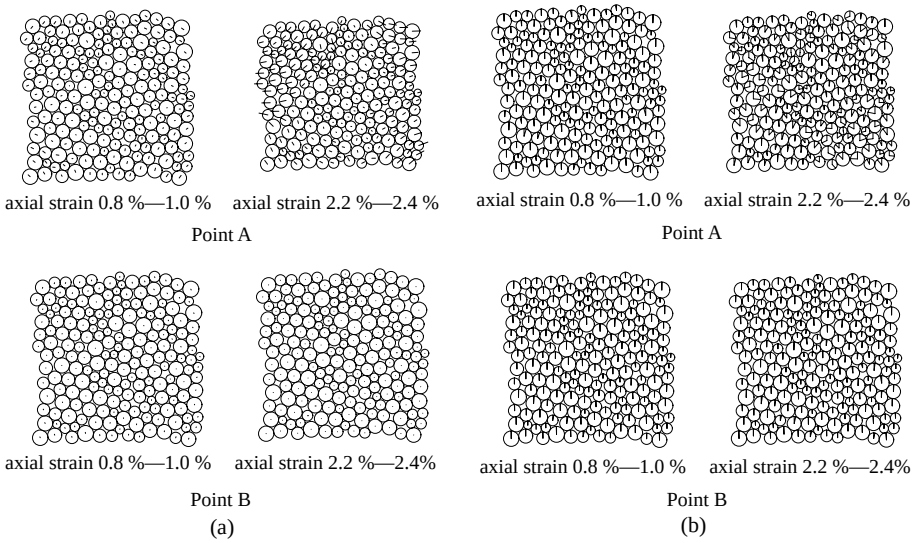

Fig. 14. Motion of particles in unit cells located at Points A and B: (a) velocity of particles and (b) rotation rate of particles.

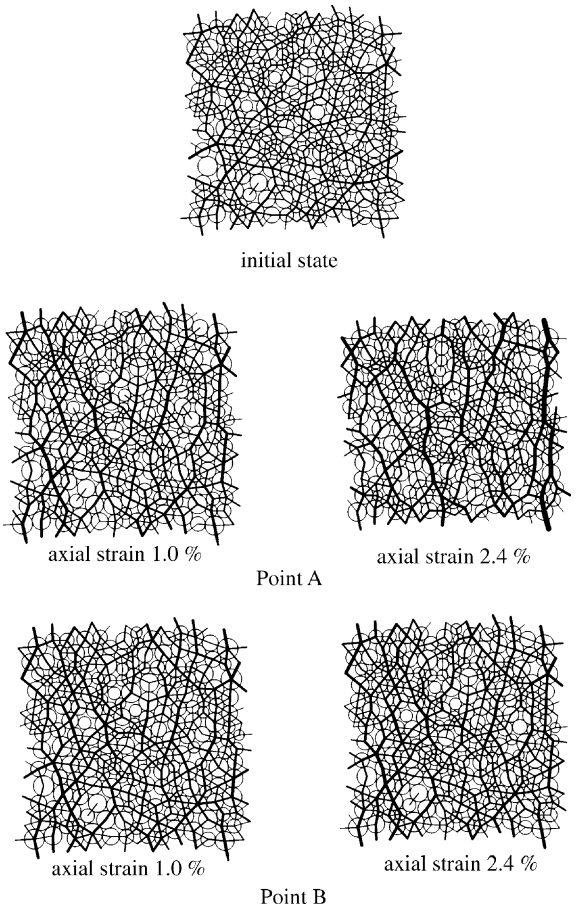

Fig. 15. Distribution of normal contact force in unit cells located at Points A and B.

As can be seen from these figures, the proposed global–local analysis method enables us to characterize the mechanical behavior in unit cells that are located at macroscopic material points of the overall structure. Although this feature would be helpful to understand the micro–macro coupling phenomena, we decide to leave detailed and qualitative investigation of micro–macro coupling behavior to other opportunities because the main purpose of this paper is to propose the new two-scale or global–local analysis method for granular media.

4.3. Bending test of cohesive granular material

In order to see the effect of cohesion, we simulate a bending test of a beam-like structure composed of cohesive granular materials. The overall structure is bended by controlling displacement U at the right-hand side surface. In the simulation, the unloading is also considered to demonstrate the irreversible character of the deformation.

The finite element model of the macroscopic structure under consideration is shown in Fig. 16, and the unit cell model is the same as that in Section 4.2 (Fig. 9(b)). Cohesion is given randomly to contact points so that the average value is $c_n = c_t = 0.1$ MPa. To have the initial arrangement of particles, hydrostatic

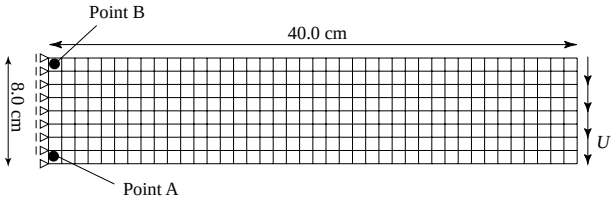

Fig. 16. Macroscopic structure under bending.

pressure of 0.1 MPa is uniformly applied to the unit cell. After the resulting initial stress in the cell is removed, the actual global–local analysis is performed. The other physical constants used in this simulation are given as follows: the normal spring constant $s_n = 1.0 \times 10^5$ N/m, the corresponding tangential one $s_t = 7.0 \times 10^4$ N/m, the friction angle $\phi = 25°$.

Fig. 17 shows the load versus displacement curve, in which the load parameter is defined as a norm of a reaction force vector at the point C shown in Fig. 16. We can see that the curve tends to exhibit linearity up to some level of macroscopic deformation in contrast to the case of noncohesive materials (see the result in Section 4.2). This is due to the fact that the onset of the nonlinear response caused by slippage between particles is delayed by the presence of cohesion. For the nonlinear response, this curve exhibits a jagged response or, equivalently, loses its smoothness. This is definitely caused by the loss of cohesion between particles in unit cells. When load parameter returns to zero, the irreversible characteristics of deformation can be observed, though the macroscopic load decreases almost linearly. Note, however, that any macroscopic constitutive model has not been introduced in this simulation.

Fig. 18 shows the distribution of the semi-norm of the deviator strain and stress with deformed configurations at loading steps (1)–(4) shown in Fig. 17. In Steps (1) and (2), the large deviator strain concentrates near the top and bottom surface of left-hand side of the specimen, while the deviator stress concentrates only near bottom surfaces. This nonsymmetric deformation about the axis of this beam-like structure indicates the difference of the responses to tensile and compressive loadings. Then, even in the final loading step (Step (4)), in which the load parameter set to zero, the heterogeneous residual stress and deviator strain remains in the specimen.

Fig. 19 shows the distribution of microcracks in the unit cells located at Points A and B given in Fig. 16, which results from the loss of cohesion between particles. This microscopic behavior causes the jagged curve given in Fig. 17 for the overall structure as well as the nonsymmetric response observed in Fig. 18. Although both Points A and B have high macroscopic strain values in Fig. 18, the former is under compression and the latter is under tension macroscopically. In Steps (1) and (2), many microcracks were

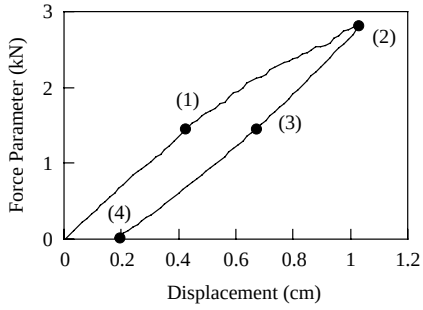

Fig. 17. Load parameter versus macroscopic displacement.

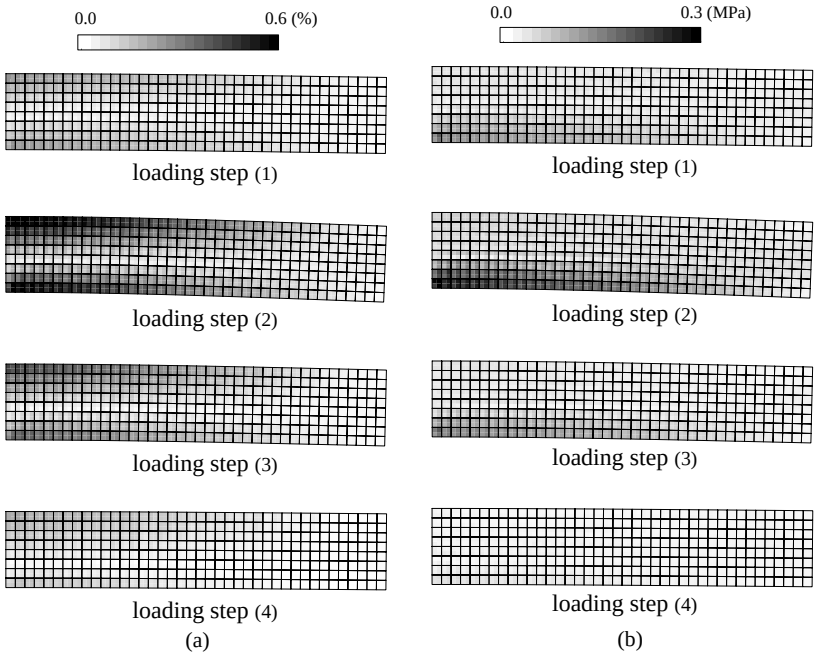

Fig. 18. Distribution of macroscopic strain and stress with deformed mesh. Norm of (a) deviator strain and (b) deviator stress.

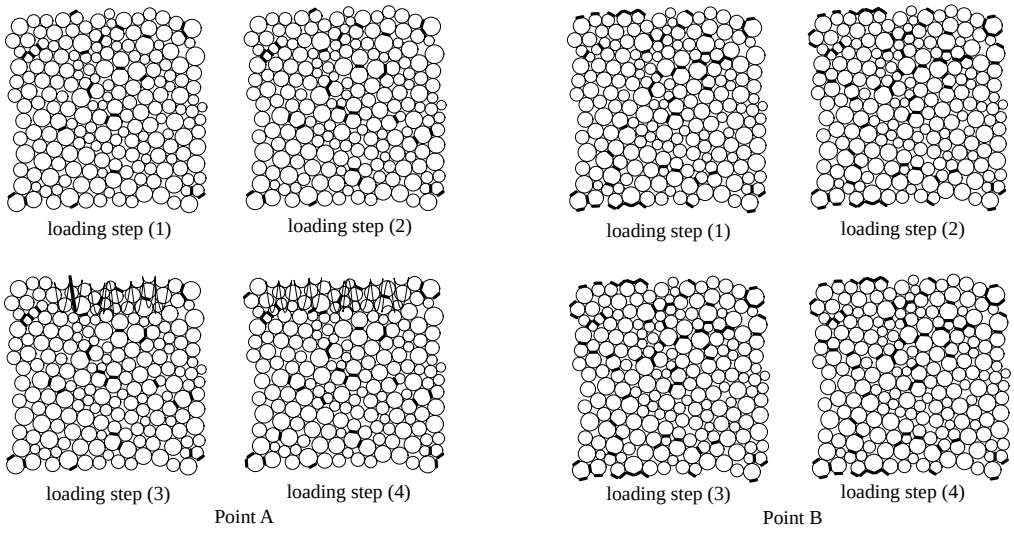

Fig. 19. Distribution of microcracks.

generated, while few microcracks are generated in Steps (2)–(4). Also, the unit cell located at Point B has more microcracks than that at Point A. Furthermore, many microcracks for Point A exhibit the opening due to tensile rupture between particles, though microcracks due to shear at contact points are predominant.

By taking the cohesion between particles into consideration, we can simulate the peculiar macroscopic deformation characteristics resulting from the generation of microcracks in the microstructure.

5. Concluding remarks

Tremendous amounts of research have been made on the modeling of the macroscopic or phenomenological constitutive laws for granular media. Some of them are incorporated with the microscale mechanism of particle motion with reference to micromechanics. However, such prior attempts have been inconclusive. In this context, the multiple scale modeling have been receiving increasing attention in both theoretical and computational mechanics. The two-scale modeling employed in this paper is based on the mathematical homogenization theory for quasi-static equilibrium problems for granular media.

In the proposed global–local analysis method, we prepare the geometrical and physical information about the microstructures that can reproduce the macroscale material response after averaging the microscale structural responses. Therefore, it is not necessary to have a priori the knowledge of the macroscopic or phenomenological material behavior that is usually given as a constitutive law. Such a way of thinking is applicable to various kinds of heterogeneous media. One of the typical applications is the present development for granular media. In the area of computational mechanics, this study must have been the first trial to incorporate the microscopic particulate nature into the global–local computations.

Nonetheless, there are some difficulties in modeling the higher order nonlinearities such as nonlocal effects of deformation. For example, the proposed method cannot simulate the formation of macroscale slip lines or so-called shear bands caused by macroscopic strain localization. The theoretical and algorithmic developments for simulating such peculiar mechanical behavior should be one of our future studies.

Appendix A. Granular element method for microscale problems

We review the formulation of the GEM with reference to Kishino (1989), which would provide the equivalent solution for microscopic problem (23). After providing the constitutive equation with constraint conditions and the equilibrium equation of a single particle, we derive the equilibrium equation with the periodic boundary conditions for unit cells (granular assembly). For our notational convenience to describe the GEM, all the tensor quantities are represented in vector or matrix forms expressed by $\{\cdot\}$ or $[\cdot]$.

A.1. Constitutive relation for particle contacts

We first introduce the constitutive equation and the constraint conditions for particle contacts. Let rigid circular particles i and j be in contact with each other on contact point C^{ij}. The unit normal vector of particle i toward particle j on C^{ij} and the corresponding tangent one are respectively given by

$$\boldsymbol{n}^{ij} = \frac{\boldsymbol{y}^j - \boldsymbol{y}^i}{|\boldsymbol{y}^j - \boldsymbol{y}^i|} \quad \text{and} \quad \boldsymbol{t}^{ij} = \begin{Bmatrix} -n_2^{ij} \\ n_1^{ij} \end{Bmatrix}, \tag{A.1}$$

where $\boldsymbol{y}^i$ and $\boldsymbol{y}^j$ are the position vectors of the center points of these particles. The kinetic variable on C^{ij} is the contact force $\{T^{ij}\} = \{T_{\mathrm{n}}^{ij}, T_{\mathrm{t}}^{ij}\}^{\mathrm{T}}$, whereas the kinematic variable associated with $\{T^{ij}\}$ in the constitutive equation is the relative displacement $\{[[u^{ij}]]\} = \{[[u_{\mathrm{n}}^{ij}]], [[u_{\mathrm{t}}^{ij}]]\}^{\mathrm{T}}$ between two particles. Here, subscripts n and t respectively represent the normal and tangential components of variables, which refer to the local coordinate system whose base vectors are $\{n^{ij}\} := \boldsymbol{n}^{ij}$ and $\{t^{ij}\} := \boldsymbol{t}^{ij}$.

In the GEM, the elastic characteristics of a continuum are replaced by those of the spring devices at contact points. We employ the normal and tangential spring devices on contact point C^{ij} as shown in Fig. 20(a). Then, we have the following simple linear relationship between $\{T^{ij}\}$ and $\{[[u^{ij}]]\}$:

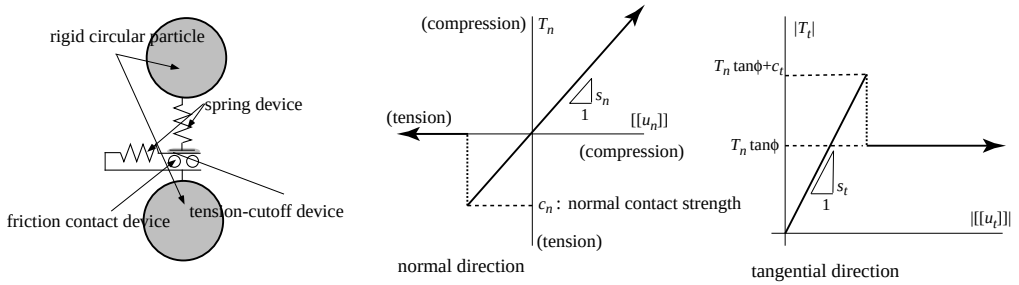

Fig. 20. Illustration of the constitutive relation for particle contacts. (a) Illustration of the constitutive model and (b) constitutive behavior for a contact point.

$$\{T^{ij}\} = [S]\{[[u^{ij}]]\}, \tag{A.2}$$

where $[S]$ is the elastic modulus matrix given as

$$[S] = \begin{bmatrix} s_{\mathrm{n}} & 0 \\ 0 & s_{\mathrm{t}} \end{bmatrix}.$$

Here, s_{n} and s_{t} are the elastic constants in the normal and tangential directions, respectively.

Remark A.1. According to the Hertz's contact theory with respect to the normal direction and Mindlin's theory with respect to the tangential one (see, e.g., Mindlin, 1949; Johnson, 1985; Oda and Iwashita, 1999), the elastic moduli are not constant on a contact area, which is actually a point in our modeling. However, since the elastic constants s_{n} and s_{t} are sufficiently stiff, $[[u^{ij}_{\mathrm{n}}]]$ must be small enough. Thus, the above linear constitutive law (A.2) would be a relevant approximation.

In order to express the slip between particles, we set up the frictional contact device as illustrated in Fig. 20(a). Then the contact condition on C^{ij} is expressed as

$$[[u^{ij}_{\mathrm{n}}]] = 0. \tag{A.3}$$

When this condition does not hold, we set zero to the contact force vector. Also, the friction condition between particles has been given in (9) and is rewritten as

$$|T^{ij}_{\mathrm{t}}| \leqslant -T^{ij}_{\mathrm{n}} \tan\phi, \tag{A.4}$$

which is known as the Mohr–Coulomb's friction condition. If the tangential component of the contact force violates this condition, we correct it compulsively to the following limit value:

$$T'^{ij}_{\mathrm{t}} = \mathrm{sign}(T^{ij}_{\mathrm{t}})(-T^{ij}_{\mathrm{n}} \tan\phi), \tag{A.5}$$

where ϕ is the friction angle on C^{ij} and $\mathrm{sign}(\cdot)$ provides the sign of a scalar quantity $\cdot$.

Although original GEM can simulate only dry granular materials, we here introduce the cohesive condition for cohesive granular materials such as rocks and stones. In this study, we employ the tension-cutoff device that resists to tensile forces to some extent and assume the following cohesive conditions:

$$\begin{cases} T^{ij}_{\mathrm{n}} \leqslant -c_{\mathrm{n}}, \\ |T^{ij}_{\mathrm{t}}| \leqslant -T^{ij}_{\mathrm{n}} \tan\phi + c_{\mathrm{t}}, \end{cases} \tag{A.6}$$

where c_{n} and c_{t} are the normal and tangential component of cohesion, respectively. In other words, they are normal and tangential contact strength. This contact model is called bonded-particle model and well used

to the simulation of rocks (see, e.g., Hazzard and Young, 2000). When the normal cohesive condition is not satisfied, we set zero to the contact force vector, c_n and c_t compulsively. When the tangential cohesive condition is not satisfied, c_n and c_t are set to zero. The contact behavior in GEM is summarized in Fig. 20(b).

A.2. Equilibrium equation of a particle

Let us consider the quasi-static equilibrium of a single particle i whose radii is given by r^i as shown in Fig. 21. The translational equilibrium for particle i is given by

$$\sum_{j=1}^{\alpha} \{F^{ij}\} = \{0\}, \tag{A.7}$$

where $\{F^{ij}\}$ is the translational force exerted on i by any particle j, which is in contact with i on a contact point C^{ij}, and α is the total number of particles in contact with i. The rotational equilibrium of particle i takes the form

$$\sum_{j=1}^{\alpha} M^{ij} = 0, \tag{A.8}$$

where M^{ij} is the moment of a contact force exerted by j. The equilibrium equations (A.7) and (A.8) can be combined as

$$\sum_{j=1}^{\alpha} \{f^{ij}\} = \{0\}; \qquad \{f^{ij}\} = \left\{F_1^{ij}, F_2^{ij}, M^{ij}/r^i\right\}^{\mathrm{T}}, \tag{A.9}$$

where $\{f^{ij}\}$ is the generalized force vector for a single contact point C^{ij}.

The generalized force vector $\{f^{ij}\}$ defined in Cartesian axis $\boldsymbol{y}_1, \boldsymbol{y}_2$, are related to the contact force vector $\{T^{ij}\}$ through the coordinate transformation matrix $[R^{ij}]$ via

$$\{f^{ij}\} = [R^{ij}]\{T^{ij}\}. \tag{A.10}$$

Here, the components of $[R^{ij}]$ are given by

$$[R^{ij}] = \begin{bmatrix} n_1^{ij} & -n_2^{ij} \\ n_2^{ij} & n_1^{ij} \\ 0 & 1 \end{bmatrix}. \tag{A.11}$$

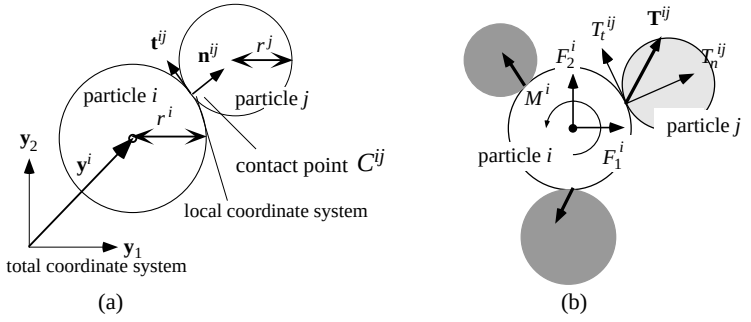

Fig. 21. Coordinate systems and kinetic variables: (a) total and local coordinate systems and (b) contact forces and generalized forces.

Using Eq. (A.10), we can rewrite the equilibrium equation (A.9) for particle i as follows:

$$\sum_{j=1}^{\alpha}([R^{ij}]\{T^{ij}\}) = \{0\}. \tag{A.12}$$

Since the motion of each particle is constrained from friction and contact on contact point C^{ij}, the microscopic analysis is always nonlinear. Thus, we replace the quasi-static equilibrium equation (A.12) by the rate form as

$$\sum_{j=1}^{\alpha}([R^{ij}]\{\dot{T}^{ij}\}) = \{0\}. \tag{A.13}$$

The kinematic variables of the particle motion are the translational displacements, u_1^i and u_2^i, and the rotation ω^i of particle i. Putting them into a generalized element displacement vector such that $\{u^i\} = \{u_1^i, u_2^i, r^i\omega^i\}^{\mathrm{T}}$, we shall use their rates to be consistent with rate form (A.13). Then, the relationship between the relative velocity $\{[[\dot{u}^{ij}]]\}$ on C^{ij} and the generalized element velocities $\{\dot{u}^i\}$ and $\{\dot{u}^j\}$ are given as follows:

$$\left\{[[\dot{u}^{ij}]]\right\} = -[R^{ij}]^{\mathrm{T}}\{\dot{u}^i\} + [\hat{R}^{ij}]^{\mathrm{T}}\{\dot{u}^j\}, \tag{A.14}$$

where

$$[\hat{R}^{ij}] = \begin{bmatrix} n_1^{ij} & -n_2^{ij} \\ n_2^{ij} & n_1^{ij} \\ 0 & -1 \end{bmatrix}.$$

Finally, using the linear constitutive law (A.2) and the generalized velocity–relative velocity relation (A.14), we can rewrite the rate form of the equilibrium equation (A.13) for particle i as follows:

$$\sum_{j=1}^{\alpha}([R^{ij}]\{T^{ij}\}) = [k^{ii}]\{\dot{u}^i\} - \sum_{j=1}^{\alpha}([\hat{k}^{ij}]\{\dot{u}^j\}) = \{0\}, \tag{A.15}$$

where

$$[k^{ii}] = \sum_{j=1}^{\alpha}\left([R^{ij}][S][R^{ij}]^{\mathrm{T}}\right) \quad \text{and} \quad [\hat{k}^{ij}] = [R^{ij}][S][\hat{R}^{ij}]^{\mathrm{T}}.$$

A.3. Treatment of periodic boundary condition

We here introduce the periodic boundary condition to the GEM formulation. Fig. 22 schematically shows the periodicity of a unit cell with respect to adjacent cells. Here, due to the periodicity, particle $\bar{i}$ in one of the adjacent cells is identified with particle i in this unit cell. We call this particle i the master particle whereas $\bar{i}$ the slave particle. The microscopic displacement vectors of these particles are respectively expressed as follows:

$$\{u^i\} = [E]\{y^i\} + \{u^{i1}\}, \tag{A.16}$$

$$\{u^{\bar{i}}\} = [E]\{y^{\bar{i}}\} + \{u^{\bar{i}1}\}, \tag{A.17}$$

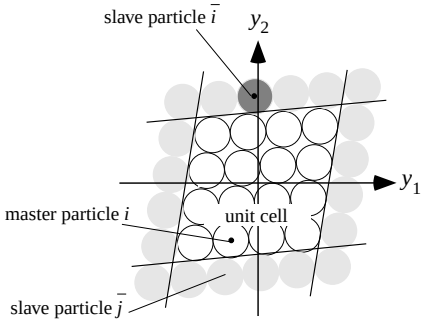

Fig. 22. Master and slave particles for periodic motion.

each of which is equivalent to (29). Here, $[E] := \boldsymbol{E}$ is the macroscopic (average) strain matrix, and $\{u^{i1}\}$ and $\{u^{\bar{i}1}\}$ are the Y-periodic displacement vectors of i and $\bar{i}$, respectively. Then the periodic boundary condition is expressed as

$$\{u^{i1}\} = \{u^{\bar{i}1}\}. \tag{A.18}$$

Subtracting (A.16) from (A.17) with (A.18), we have

$$\{u^{\bar{i}}\} = \{u^{i}\} + [E](\{y^{\bar{i}}\} - \{y^{i}\}). \tag{A.19}$$

If master particle i is in contact with α particles containing $\bar{\alpha}$ slave particles, the last term in the left-hand side of the equilibrium equation (A.15) for master particle i is divided into the parts about the master particles and slave ones and Eq. (A.15) yields

$$[k^{ii}]\{\dot{\boldsymbol{u}}^{i}\} - \sum_{j=1}^{\alpha-\bar{\alpha}}([\hat{\boldsymbol{k}}^{ij}]\{\dot{\boldsymbol{u}}^{j}\}) - \sum_{j=1+\alpha-\bar{\alpha}}^{\alpha}([\hat{\boldsymbol{k}}^{i\bar{j}}]\{\dot{\boldsymbol{u}}^{\bar{j}}\}) = \{0\}, \tag{A.20}$$

in which the last term in the left-hand side is due to the periodicity constraint for particle i with respect to slave particles. Here, $[k^{ii}]$ is rewritten as following expression:

$$[k^{ii}] = \sum_{j=1}^{\alpha-\bar{\alpha}}\left([R^{ij}][S][R^{ij}]^{\mathrm{T}}\right) + \sum_{j=1+\alpha-\bar{\alpha}}^{\alpha}\left([R^{i\bar{j}}][S][R^{i\bar{j}}]^{\mathrm{T}}\right).$$

Then, by substituting the rate forms of (A.19) into the last term in the left-hand side in (A.20) with some algebraic manipulations, we arrive at the following equilibrium equation for a single particle i with the periodicity constraint associated with slave particles:

$$\{\dot{\boldsymbol{H}}^{i}\} = [k^{ii}]\{\dot{\boldsymbol{u}}^{i}\} - \sum_{j=1}^{\alpha-\bar{\alpha}}([\hat{\boldsymbol{k}}^{ij}]\{\dot{\boldsymbol{u}}^{j}\}) - \sum_{j=1+\alpha-\bar{\alpha}}^{\alpha}([\hat{\boldsymbol{k}}^{i\bar{j}}]\{\dot{\boldsymbol{u}}^{j}\}) = [K^{i}]\{\dot{\boldsymbol{u}}^{ij}\}, \tag{A.21}$$

where the components of the element stiffness matrix $[K^{i}]$ and the displacement vector $\{\dot{\boldsymbol{u}}^{ij}\}$ is given by

$$[K^{i}] = \left[\,[k^{ii}] \quad -[\hat{\boldsymbol{k}}^{i1}] \quad \cdots \quad -[\hat{\boldsymbol{k}}^{i\bar{j}}] \quad \cdots \quad -[\hat{\boldsymbol{k}}^{i\bar{\alpha}}]\,\right],$$

$$\{\dot{\boldsymbol{u}}^{ij}\} = \left\{\{\dot{\boldsymbol{u}}^{i}\}^{\mathrm{T}}, \{\dot{\boldsymbol{u}}^{1}\}^{\mathrm{T}}, \ldots, \{\dot{\boldsymbol{u}}^{j}\}^{\mathrm{T}}, \ldots, \{\dot{\boldsymbol{u}}^{\alpha}\}^{\mathrm{T}}\right\}^{\mathrm{T}}.$$

And, here, we have defined the vector of external forces as

$$\{\dot{H}^i\} = [\dot{E}] \sum_{j=1+\alpha-\bar{\alpha}}^{\alpha} [\hat{k}^{i\bar{j}}](\{y^{\bar{j}}\} - \{y^j\}). \tag{A.22}$$

Finally, if there are n particles in the unit cell, we define the overall external force vector and the overall generalized velocity vector for all the particles as

$$\{\dot{H}\} = \left\{\{\dot{H}^1\}^{\mathrm{T}}, \ldots, \{\dot{H}^i\}^{\mathrm{T}}, \ldots, \{\dot{H}^j\}^{\mathrm{T}}, \ldots, \{\dot{H}^n\}^{\mathrm{T}}\right\}^{\mathrm{T}},$$

$$\{\dot{u}\} = \left\{\{\dot{u}^1\}^{\mathrm{T}}, \ldots, \{\dot{u}^i\}^{\mathrm{T}}, \ldots, \{\dot{u}^j\}^{\mathrm{T}}, \ldots, \{\dot{u}^n\}^{\mathrm{T}}\right\}^{\mathrm{T}}.$$

Then, by piling up the equilibrium equations (A.21) according to the order of $\{\dot{u}\}$ for all the particles within a unit cell except for the slave particles, which enjoy the periodicity constraints, we have the rate form of the equilibrium equation for the unit cell as

$$\{\dot{H}\} = [K]\{\dot{u}\}, \tag{A.23}$$

which should be solved for the overall generalized velocity vector $\{\dot{u}\}$, where $[K]$ is the overall stiffness matrix, which consists of the element stiffness $[K^i]$ of all the particles with reference to the order of $\{\dot{u}\}$. The components of $[K]$ is given by

$$[K] = \begin{bmatrix} [k^{11}] & \cdots & -[\hat{k}^{1i}] & \cdots & -[\hat{k}^{1\bar{j}}] & \cdots & -[\hat{k}^{1n}] \\ \cdots & \ddots & \cdots & \cdots & \cdots & \cdots & \cdots \\ -[\hat{k}^{i1}] & \cdots & [k^{ii}] & \cdots & -[\hat{k}^{ij}] & \cdots & -[\hat{k}^{in}] \\ \cdots & \cdots & \cdots & \ddots & \cdots & \cdots & \cdots \\ -[\hat{k}^{\bar{j}1}] & \cdots & -[\hat{k}^{\bar{j}i}] & \cdots & [k^{jj}] & \cdots & -[\hat{k}^{jn}] \\ \cdots & \cdots & \cdots & \cdots & \cdots & \ddots & \cdots \\ -[\hat{k}^{n1}] & \cdots & -[\hat{k}^{ni}] & \cdots & -[\hat{k}^{nj}] & \cdots & [k^{nn}] \end{bmatrix}.$$

We here note that the nondiagonal block $-[\hat{k}^{ij}]$ should be a zero-matrix if particles i and j do not contact with each other.

References

Allaire, G., 1992. Homogenization and two-scale convergence. SIAM J. Math. Anal. 23, 1482–1518.

Benssousan, A., Lions, J.L., Papanicolaou, G., 1978. Asymptotic Analysis for Periodic Structures. North Holland, Amsterdam.

Cundall, P.A., Strack, O.D.L., 1979. A discrete numerical model for granular assemblies. Géotechnique 29, 47–65.

Emeriault, F., Cambou, B., Mahboubi, A., 1996. Homogenization for granular materials: non-reversible behavior. Mech. Cohes.-Frict. Mater. 1, 199–218.

Ghosh, S., Moorthy, S., 1995. Elastic–plastic analysis of arbitrary heterogeneous materials with the Voronoi cell finite element method. Comput. Meth. Appl. Mech. Engrg. 121, 373–409.

Hazzard, J.F., Young, R.P., 2000. Simulating acoustic emission in bonded-particle models of rock. Int. J. Rock Mech. Min. Sci. 37, 867–872.

Johnson, K.L., 1985. Contact Mechanics. Cambridge University Press, Cambridge.

Kikuchi, N., Oden, J.T., 1988. Contact Problem in Elasticity: A Study of Variational Inequalities and Finite Element Methods. SIAM, Philadelphia.

Kishino, Y., 1989. Computer Analysis of Dissipation Mechanism in Granular Media. Powders and Grains. A.A. Balkema, Rotterdam, pp. 323–330.

Kuhn, M.R., 1999. Structured deformation in granular materials. Mech. Mater. 31, 407–429.
Liao, C.L., Chan, T.C., Suiker, A.S.J., Chang, C.S., 2000. Pressure-dependent elastic moduli of granular materials. Int. J. Numer. Anal. Meth. Geomech. 24, 265–279.
Lions, J.L., 1981. Some Methods in the Mathematical Analysis of Systems and Their Control. Science Press, Beijing, China.
Mindlin, R.D., 1949. Compliance of elastic bodies in contact. Trans. ASME, J. Appl. Mech. 16, 259–269.
Nemat-Nasser, S., 2000. A micromechanically-based constitutive model for frictional deformation of granular materials. J. Mech. Phys. Solids 48, 1541–1563.
Oda, M., Iwashita, K. (Eds.), 1999. Mechanics of Granular Materials: An Introduction. A.A. Balkema, Rotterdam.
Sanchez-Palencia, E., 1980. Non-homogeneous Media and Vibration Theory. In: Lecture Notes in Physics 127. Springer-Verlag, Berlin.
Swan, C.C., Cakmak, A.S., 1994. A hardening orthotropic plasticity model for non-frictional composites: rate formulation and integration algorithm. Int. J. Numer. Meth. Engrg. 37, 839–860.
Terada, K., Kikuchi, N., 2001. A class of general algorithms for nonlinear multi-scale analyses of heterogeneous media. Comput. Meth. Appl. Mech. Engrg. 190, 5427–5464.
Wren, J.R., Borja, R.I., 1997. Micromechanics of granular media, Part II: Overall tangential moduli and localization model for periodic assemblies of circular disks. Comput. Meth. Appl. Mech. Engrg. 141, 221–246.